# Toward Understanding the Occurrence of Both Wet and Dry Sahel Seasons during El Niño: The Modulating Role of the Global Ocean

CATHERINE POMPOSI

*Department of Earth and Environmental Sciences, Columbia University, New York, New York*

YOCHANAN KUSHNIR

*Lamont-Doherty Earth Observatory, Palisades, New York*

ALESSANDRA GIANNINI

*International Research Institute for Climate and Society, The Earth Institute at Columbia University, New York, New York*

MICHELA BIASUTTI

*Lamont-Doherty Earth Observatory, Palisades, New York*

(Manuscript received 26 March 2019, in final form 7 October 2019)

ABSTRACT

Prior research has shown that dry conditions tend to persist in the Sahel when El Niño develops. Yet, during the historic 2015 El Niño, Sahel summer precipitation was anomalously high, particularly in the second half of the season. This seeming inconsistency motivates a reexamination of the variability of precipitation during recent El Niño years. We identify and composite around two different outcomes for Sahel summer season: an anomalously wet season or an anomalously dry season as El Niño develops to its peak conditions over the observational record spanning 1950–2015. We find consistently cool temperatures across the global tropics outside the Niño-3.4 region when the Sahel is anomalously wet during El Niño years and a lack of cooling throughout the tropics when the Sahel is anomalously dry. The striking differences in oceanic surface temperatures between wet years and dry years are consistent with a rearrangement of the entire global circulation in favor of increased rainfall in West Africa despite the presence of El Niño.

## 1. Introduction

The semiarid narrow strip of land located directly south of the Sahara Desert known as the Sahel receives the majority of its annual precipitation through the West African monsoon (WAM) system. The WAM regional circulation pattern develops in late spring, bringing moist air from the Atlantic Ocean and the Gulf of Guinea to the continent. The WAM reaches its northernmost location over the Sahel (here defined as the 10°–20°N band across the width of the continent) in boreal summer [July–September (JAS)]. Recently, variability in the WAM system imposes a range of 300–800 mm in seasonal precipitation accumulation (Nicholson and Webster 2007) that has been shown to strongly covary with global patterns of sea surface temperature (SST) departure from climatology (hereinafter SST anomalies), in the Atlantic, Pacific, and Indian Ocean basins (Lamb 1978; Folland et al. 1986; Rowell et al. 1995; Biasutti et al. 2008). Multiple studies with atmospheric general circulation models (AGCMs) driven with observed SSTs capture both low-frequency (i.e., decadal) and high-frequency (i.e., interannual) variations of Sahel rainfall, thus confirming that their primary driver is the state of the upper global ocean temperature (Palmer 1986; Giannini et al. 2003; Zhang and Delworth 2006; Bader and Latif 2003; Lu 2009).

Supplemental information related to this paper is available at the Journals Online website: https://doi.org/10.1175/JCLI-D-19-0219.s1.

*Corresponding author*: Catherine Pomposi, cap2203@columbia.edu

DOI: 10.1175/JCLI-D-19-0219.1

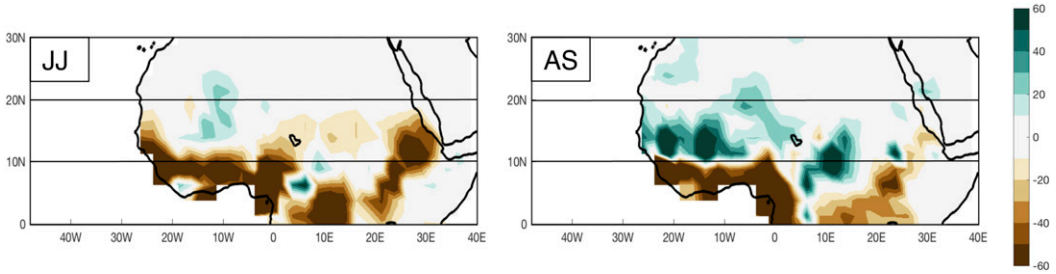


FIG. 1. 2015 Sahel seasonal anomaly (mm month$^{-1}$) from GPCC (climatologic period 1979–2008) for (left) JJ and (right) AS. Black horizontal lines distinguish Sahel latitudes (10°–20°N).

On interannual time scales, a dominant oceanic driver of Sahel precipitation variability is the El Niño–Southern Oscillation (ENSO) phenomenon (Rowell et al. 1995; Janicot et al. 1996; Ward 1998; Thiaw et al. 1999). A negative correlation between ENSO and rainfall in the Sahel indicates that the warm conditions in the eastern tropical Pacific characteristic of El Niño are linked to reduced precipitation over the region (Janicot et al. 1996; Rowell et al. 1992; Janicot et al. 2001). Theoretical consideration suggests that the warming of the upper ocean in the eastern equatorial Pacific is communicated to the atmosphere via deep convection (Gill 1980; Yulaeva and Wallace 1994; Chiang and Sobel 2002) and that the upper tropospheric heating generated by the convection is distributed horizontally throughout the tropics by Kelvin and Rossby waves. The increase in upper tropospheric temperatures imposes greater atmospheric stability and anomalous subsidence outside the area of convective heating due to El Niño (Lintner and Chiang 2005). In broad terms, regions of the ''remote tropics'' (in this case outside the eastern tropical Pacific), including the Sahel, are anomalously dry during El Niño events because this increased atmospheric stability requires reaching an increased convective threshold, one difficult to meet (Giannini et al. 2008; Neelin et al. 2003; Lyon 2004; Seth et al. 2011).

Notably, though, this framework has limited value where regional processes such as the advection of moisture play a large role (Lintner and Chiang 2005). In such case, the precipitation response to El Niño in remote regions may not be as straightforward as theory suggests. For example, during the recent historic El Niño event in 2015 observations show that the Sahel rainy season was instead anomalously wet (Fig. 1). In Fig. 1 there is some drying evident along the west coast of Africa and at the southern margin in the Sahel, as well as in the eastern part of the region during the first half of the season in June–July (JJ). Yet, particularly in areas to the west of Lake Chad, these dry anomalies are more than compensated for during August–September (AS) with anomalous precipitation rates of over 30 mm \month$^{-1}$ in most places. The strong wetting late in the season as observed in 2015 is an interesting characteristic that might be lost in a seasonally averaged viewpoint and is one of the reasons why this study largely focuses on both early and late-season behavior. Although the seasonal signature tends to be dominated by the precipitation response late in the season (see Fig. S1 and the related discussion in the online supplemental material), on a seasonal average Fig. 2 reveals that since 1950 a handful of anomalously wet Sahel summer seasons have occurred simultaneously with the development of El Niño events and that the anomalously high precipitation in the summer of 2015 was not a stand-alone case. Motivated by these findings, this study has the following objectives:

1) characterize Sahel precipitation during El Niño summers in terms of the difference between the first and second half of the season,
2) identify consistent features in the global ocean surface temperatures that help to distinguish wet El Niño years from dry El Niño years in the Sahel and determine relative risks of reduced precipitation, and
3) where differences in precipitation exist, determine whether they can be interpreted through a lens of El Niño impact in combination with the global oceanic background.

We note that, from a decision-making perspective, the expectation that El Niño tends to dry the Sahel is commonly relied upon in delivering seasonal forecasting information in forums such as the Prévisions Saisonnières en Afrique de l'Ouest (PRESAO), the World Meteorological Organization's Regional Climate Outlook Forum for West Africa. Given that this signal is prominently featured in subseasonal forecasting activities, and with a recent example of where the expected impacts did not entirely occur, revisiting the subtleties

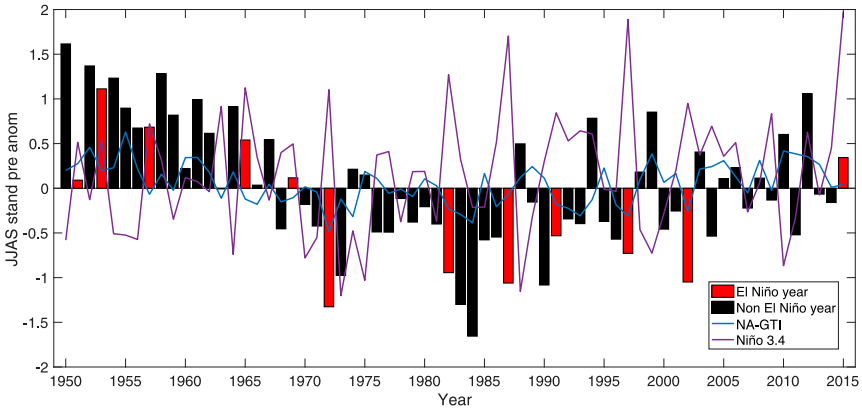


FIG. 2. West African Sahel (10°–20°N and 20°E–20°W) JJAS standardized precipitation anomalies (climatologic period 1979–2008) from GPCC (bars) categorized by type of year (El Niño in red, and non–El Niño in black), with NA-GTI (blue line) and Niño-3.4 (purple line).

in precipitation response during recent El Niño events is fitting.

On the basis of current understanding of the major oceanic drivers of precipitation in the Sahel, we seek to compare North Atlantic SST to conditions in the global tropics overall (where the El Niño signal naturally plays a large role) and determine if this helps to distinguish wet from dry El Niño years. We also look into the likelihood that having a precipitation season with lower than normal totals, even in El Niño years, may differ given the configuration of additional oceanic drivers. Notably, within the observational design of the present study, additional influences of individual basins like the Mediterranean Sea (Gaetani et al. 2010; Park et al. 2016; Rowell 2003) or Indian Ocean (Hagos and Cook 2008) cannot be explicitly quantified. However, in the case of the Indian Ocean, its role will naturally be incorporated in some part into the near-global index we propose using.

## 2. Methods and data

### a. Data

The precipitation data used for the study are from the World Climate Research Programme's Global Precipitation Climatology Centre (GPCC), version 7, dataset. The full research product has coverage from 1901 to 2013 on a global 2.5° latitude/longitude grid (Becker et al. 2013). This dataset is chosen because of its longer time of record, but we focus primarily on the time period of 1950–2013 because of the lack of station data feeding into the product for the Sahel prior to 1950. Because the full research product ends in 2013, we utilize NASA's Global Precipitation Climatology Project (GPCP) monthly dataset, version 2.2, for 2014 and 2015. GPCP combines observations and satellite retrievals to provide precipitation data on a global 2.5° latitude/longitude grid (Adler et al. 2003). To ensure that we are studying a true difference in signal for wet and dry years, we only retain years in the analysis in which the GPCC standardized precipitation anomaly matches in sign to another observed rainfall product used extensively in Sahel precipitation studies, the University of East Anglia's Climatic Research Unit (CRU) TS 3.2 dataset. This is a commonly used precipitation product based on rain gauge measurements interpolated to a 0.5° latitude/longitude grid (Harris et al. 2014). Obtaining accurate precipitation data over the Sahel remains challenging, and previous works have attempted to distinguish the skill or limitations of various data products for the region. Given our goal to understand broad, regional characteristics on a monthly time scale and the requirement to utilize a data product spanning the twentieth century, GPCC is a reasonable product to use and shows good agreement with a regional gauge network analysis as documented in Ali et al. (2005). According to Nicholson et al. (2003), GPCC is also the most widely used observational dataset to study African precipitation characteristics. It shows a small bias error (~3%–4%) when compared to other seasonal rainfall estimates using local gauge networks (Nicholson et al. 2003). The GPCC dataset is useful here to employ, noting its longer time record than other products (specifically GPCP).

Sea surface temperature (SST) data for the time period 1950–2015 are from NOAA's Extended Reconstructed Sea Surface Temperature (ERSST) dataset, version 4 (Huang et al. 2015). The North Atlantic–global tropics index (NA-GTI) is calculated by subtracting the average anomaly across the global tropics (20°N–20°S, 180°W–180°E) from the average anomaly in the subtropical North Atlantic (10°–40°N, 75°–15°W), consistent with Giannini et al. (2013).

Atmospheric variables including moisture flux, moisture convergence, and sea level pressure are explored using the National Centers for Environmental Prediction (NCEP)–National Center for Atmospheric Research (NCAR) reanalysis (Kalnay et al. 1996), which has temporal coverage from 1948 onward and on 2.5° latitude/longitude grids.

### b. Compositing methods

To form the composites studied in this work, there are several steps. First, El Niño events during 1950–2015, characterized by warm conditions above +0.5°C for the oceanic Niño index (ONI; 3-month running average of ERSST anomalies in the Niño-3.4 region), are identified. Each individual El Niño event spans parts of two calendar years, which we will refer to as year (0)–year (1) [e.g., the 1997 (year 0)–1998 (year 1) El Niño event]. We retain only years in which El Niño conditions are in place by JAS year (0) according to the National Oceanic and Atmospheric Administration Climate Prediction Center (NOAA CPC). This results in 15 El Niño events: 1951/52, 1953/54, 1957/58, 1963/64, 1965/66, 1969/70, 1972/73, 1982/83, 1987/88, 1991/92, 1997/98, 2002/03, 2004/05, 2009/10, and 2015/16.

Since the Sahel rainy season occurs approximately 6 months prior to El Niño peak conditions and is influenced by it during ENSO development (Joly and Voldoire 2009), the behavior of rainfall during June–September (JJAS) of year (0) is studied. Of all El Niño year (0) years, we composite around positive or negative JJAS precipitation anomaly averaged over the West African Sahel (10°–20°N, 20°E–20°W), only retaining years when the standardized precipitation anomaly matches sign in the two observational datasets. This leads to two composites:

1) El Niño/wet Sahel (ENWS): 1951, 1953, 1957, 1965, 1969, 2015 ($n = 6$) and
2) El Niño/dry Sahel (ENDS): 1972, 1982, 1987, 1991, 1997, 2002 ($n = 6$).

Standardized anomalies are computed with respect to the 1979–2008 climatology and are presented as averages over the early part of the season (i.e., JJ) and the late part of the season (i.e., AS). A recent climatologic period is chosen to better frame precipitation changes compared to the recent past, as is done typically by individuals who monitor rainfall occurrence on seasonal and interannual time scales. Thus, this same period is most appropriate for us to organize our analysis around in the hopes that our research results will be practically meaningful for application in the region. To ensure the robustness of our results however, we have validated the conclusions in the following ways: 1) using a 1950–2015 climatologic period, 2) considering composites composed of all El Niño years dating back to 1901, and 3) considering composites composed of all El Niño years dating back to 1901 and only whose precipitation anomalies are above 0.5 standard deviations. Results are qualitatively similar to those presented in the paper for all of the cases described above.

### c. Model output

The ensemble mean precipitation output from model runs using the NCAR Community Atmosphere Model, version 5 (CAM5) (Neale et al. 2012), is also briefly utilized. CAM5 was forced with global historic SSTs (known as the GOGA configuration, for global ocean global atmosphere) in a multi-ensemble member long run spanning the entire twentieth century and run through 2016. A total of 16 ensemble members are produced that each differ slightly in their initial atmospheric conditions. For more information regarding these model experiments and their prior use in Sahel precipitation studies, the reader is referred to Pomposi et al. (2015, 2016). In Pomposi et al. (2016), we validate the CAM5 simulation of Sahel precipitation characteristics given SST forcing and show that CAM5 exhibits a slight wet bias but realistic median precipitation rate and range, compared to several observational data products. More recent published work (e.g., Dyer et al. 2017) has also utilized ocean-driven CAM5 model output for study and notes also the good agreement between CAM5 precipitation estimates and observations. In addition, Giannini and Kaplan (2019) show that the coupled version of the model (CESM) reproduces the relationship with the North Atlantic relative index explored here well in both the preindustrial and the historical simulation in CMIP5 (see their supplementary materials).

### d. Precipitation distribution

To determine the precipitation sensitivity to oceanic patterns, probability density functions (PDFs) and cumulative distribution functions (CDFs) are fit to output from CAM5. We note that this task would be difficult using observations given the small sample size of each composite, so model output is employed for this part of the analysis. Each PDF and CDF is constructed by using all available ensemble member output for years that are determined El Niño years (as indicated above) and then further subdivided into categories based on the sign (i.e., positive or negative) of the NA-GTI. The PDFs were constructed using Matlab software, with a nonparametric kernel density estimator that was made at every 100 points covering

TABLE 1. Summary of the sign of the Sahel precipitation anomaly, sign of the North Atlantic–global tropical index, and sign of the Niño-3.4 index for each of the years composing the composites in the study. Note that the same data are represented graphically in Fig. 2.

| Year | Sahel precipitation anomaly | NA-GTI | Niño-3.4 |
|---|---|---|---|
| 1951 | + | + | + |
| 1953 | + | + | + |
| 1957 | + | − | + |
| 1965 | + | − | + |
| 1969 | + | − | + |
| 1972 | − | − | + |
| 1982 | − | − | + |
| 1987 | − | − | + |
| 1991 | − | − | + |
| 1997 | − | − | + |
| 2002 | − | − | + |
| 2015 | + | + | + |

the data range. A normal kernel smoother was then used to smooth the PDFs.

## 3. Results

### a. Sahel rainfall and SST indices

The JJAS standardized precipitation anomalies shown in Fig. 2 display a clear and well-documented multidecadal signal overlaid with interannual variability. Figure 2 demonstrates the interplay between Sahel precipitation variability on these two key time scales. It is clear that on longer (i.e., decadal) time scales, the Sahel precipitation index largely follows the variations in the North Atlantic–global tropics SST index (NA-GTI), first introduced by Giannini et al. (2013). The NA-GTI is the difference between anomalies from 75°–15°W and 10°–40°N minus 20°S–20°N. This index was developed to reflect the current understanding of the main oceanic drivers of Sahel rainfall variability across time scales and has been shown to reconcile oceanic influence on Sahel climate in the observations, in twentieth-century SST-forced and coupled model simulations, and in the twenty-first-century projected precipitation trend (Giannini and Kaplan 2019). It relies on a framework that quantifies the competing roles of atmospheric stabilization and of moisture supply in influencing regional precipitation variability (following naming conventions in previous work; Giannini et al. 2008). The index varies from being primarily positive in the first part of the record (1950–65) then to negative (1970–95), and then switching again to positive (after 2000). This low-frequency change follows the multidecadal swing in the North Atlantic Ocean (Giannini et al. 2013). A summary of the data from Fig. 2 is also displayed in Table 1.

TABLE 2. Interannual correlations of West African Sahel standardized precipitation index (averaged over 10°–20°N and 20°E–20°W) and various SST indices for JJAS. The NA-GTI is the difference between anomalies from 75°–15°W and 10°–40°N and global 20°S–20°N. The North Atlantic–South Atlantic (NA-SA) index is calculated by subtracting anomalies in the South Atlantic (45°W–15°E and 5°–40°S) from the North Atlantic (75°–15°W and 5°–40°N). The Niño-3.4 index is the average anomaly over 5°N–5°S and 170°–120°W. The equatorial Indian (Eq Ind) index is computed by averaging anomalies over 50°–90°E, 15°S–15°N. The Mediterranean (Med) index is computed from anomalies spanning 30°–50°N, 0°–50°E. All correlations listed in the table are statistically significant (two-tailed test: $\alpha = 0.05$; degrees of freedom = 60).

| | Period | NA-GTI | NA-SA | Niño-3.4 | Eq Ind | Med |
|---|---|---|---|---|---|---|
| GPCC | 1950–2015 | 0.60 | 0.61 | −0.27 | −0.39 | 0.31 |
| CRU | 1950–2014 | 0.54 | 0.58 | −0.33 | −0.44 | 0.25 |

In addition, the figure shows a tendency for the impact of wet and dry El Niño years to also largely mimic the decadal swings. During the relatively wet 1950s–60s, all El Niño years were wet in the Sahel based on the observed standardized precipitation index, as was 2015. Of the six wet El Niño years, three occurred when the NA-GTI was positive. In contrast, for the six dry El Niño years, all occurred when the index was negative. The figure also indicates that the Sahel tends to display negative standardized precipitation anomalies when the Niño-3.4 index is positive and the NA-GTI is negative compared to when the Niño-3.4 index is positive and the NA-GTI is positive (or not strongly negative). In the latter cases, the Sahel standardized precipitation anomaly is often above 0, such as in 1951, 1953, and 2015, three of the later defined ENWS years.

Table 2 shows a summary of the correlation between the Sahel standardized precipitation index across two datasets with various SST indices. The NA-GTI shows consistently high correlation values across both datasets and also naturally takes into account the intensity of the El Niño signal as well as changes in other tropical ocean areas, such as the Indian Ocean and the tropical South Atlantic. Similarly, an index focused on only changes in the North Atlantic as compared with the South Atlantic performs well (correlations of 0.61 and 0.58 depending on precipitation dataset used), showing once more the strong correlation of this nearby basin with precipitation in the region.

### b. Anomalous rainfall in El Niño/wet Sahel and El Niño/dry Sahel composites

Figure 3 shows standardized precipitation anomalies (colors) for the two composites: El Niño/wet Sahel (ENWS) and El Niño/dry Sahel (ENDS) (for the list of years in each composite see Table 1). In each composite, we consider separately the early rainy season (JJ) and

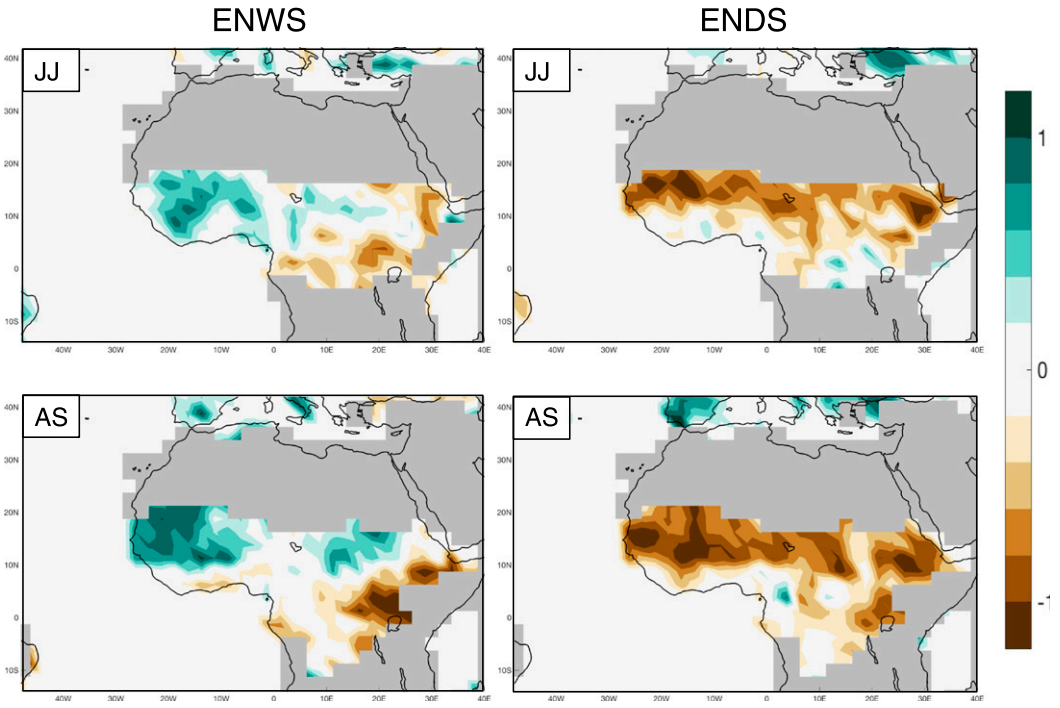


FIG. 3. Average standardized precipitation anomalies (unitless) from GPCC for (top) JJ and (bottom) AS in the (left) ENWS and (right) ENDS composites (colors). Land points are shaded in gray if the observed climatological mean does not exceed 0.5 mm day$^{-1}$.

the late rainy season (AS). Interesting contrasts in precipitation are observed between the ENWS and the ENDS composite and within the ENWS monsoon season when considering the early months (JJ) and later months (AS). Precipitation anomalies are of a similar magnitude for the ENDS composite in both JJ and AS ($\sim -0.8$ standardized units throughout much of the domain). In contrast, the wet anomalies show a clear strengthening between JJ ($\sim +0.4$ standardized units) and AS ($\sim +0.6$ to $+0.8$ standardized units). Furthermore, in the ENDS composite anomalously low precipitation is coherent across both the north–south (10°–20°N) and east–west (20°W–40°E) extent of the Sahel. This pattern is consistent with how El Niño forces anomalous moisture divergence, by suppressing uplift across the entire tropical belt outside the eastern equatorial Pacific and hence causing reduced precipitation throughout the North African sub-Saharan band (Pomposi et al. 2016). On the other hand, anomalously high precipitation rates are especially clear in the western Sahel (west of 0° longitude) in the ENWS composite. These anomalies are weakly positive in JJ and increase by AS. A similar pattern of anomalously high precipitation confined to the westernmost portion of the Sahel has been described in prior work (Dyer et al. 2017). The Sahel appears wet, particularly on its western edge, when specific humidity advection increases in response to a positive Atlantic meridional gradient (e.g., Sheen et al. 2017; Rowell 2003). That we see anomalous wetting confined to the western most Sahel only in the ENWS composite compared to the ENDS composite hints at a possibility that differences in precipitation may be influenced by SST anomaly patterns beyond El Niño. We explore this more in subsequent figures and discussion.

Figure 4 shows the frequency of occurrence of wet or dry precipitation anomalies in each 2.5° by 2.5° grid box for the respective years composing each composite. Because of the small sample size in this observational study ($n = 6$ for each composite), this is an appropriate way to display consistency in terms of sign of the anomaly and ensure that taking an overall average (as in Fig. 3) is not simply dominated by one or two particularly strong years. Interesting differences between the two composites are once more seen. For the ENDS composite, virtually all of the westernmost Sahel grid boxes show dry precipitation anomalies in four–six of the years composing the composite. There are a few grid boxes on the southern edge of the Sahel that buck this consensus with only three years dry. Overall, the drying gets stronger as the season progresses with the majority of grid boxes in the western Sahel reporting anomalously dry conditions in all six of the six years composing the composite by AS. This behavior is in

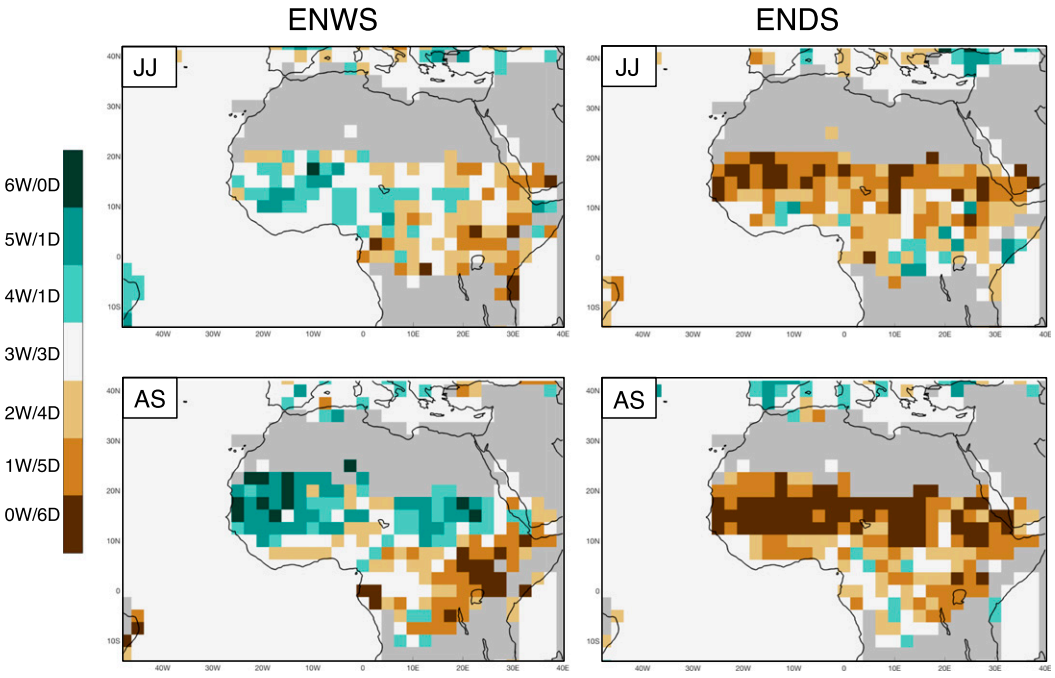


FIG. 4. Frequency of occurrence of wet and dry precipitation anomalies in each 2.5° by 2.5° grid box for the respective years composing each composite. Land points are shaded in gray if the observed climatological mean does not exceed 0.5 mm day$^{-1}$. The color bar denotes dry or wet occurrences for each composite (e.g., "6W/0D" indicates 6 wet years and 0 dry years, "5W/1D" indicates 5 wet years and 1 dry year, and so on for the years composing each composite; $n = 6$ in both cases).

clear contrast to what occurs in the ENWS composite. For one, the anomalous wetting is not nearly as spatially coherent as the drying is in the ENDS composite. Indeed, there is only a single grid box (at 10°W and 18°N) that shows anomalously wet conditions in JJ for all six years of the ENWS composite, and the wet anomaly is weaker in terms of number of years it happens (usually four) and less consistent in space. By AS, more consistency has emerged in terms of the number of grid boxes where wet conditions prevail compared to JJ. This is particularly true in the area to the west of Lake Chad. However, compared to the dry composite there are still fewer grid boxes in the ENWS composite that show a 100% wet frequency (i.e., six wet years in a 6-yr total) in this composite. Overall, the ENDS composite shows a clearer tendency for drying that is consistent both in space across the Sahel and in time (as represented by the number of years where the signal is dry) than when considering wetting in the ENWS composite.

### c. *Global SST patterns for the ENWS versus ENDS composites*

Figure 5 shows global SST anomalies for the two composites. In both composites, the clearest SST pattern is that of the warm anomalies in the central and eastern tropical Pacific, characteristic of El Niño and consistent with the design of the composite study. There are however noticeable differences between the two composites in the El Niño pattern. The largest difference is in the magnitude of SST anomalies rather than the spatial pattern. In the ENDS composite, during both JJ and AS, a narrow strip of positive SST anomalies ($>+1$°C) appears in the eastern equatorial Pacific, in contrast with the weaker warm anomalies (between +0.6° and 0.8°C) in the ENWS composite in the same region.

Another clear difference in the global SST anomaly field is the contrasting features displayed throughout the global tropics in the different composites. In the ENWS composite, the entirety of the global tropics outside the Niño region is anomalously cool, particularly the subtropical South Atlantic. The Indian Ocean basin also remains anomalously cool in JJ with the anomaly magnitude decreasing by AS. In contrast, most of the cooling in the ENDS composite is north of the equator in the Atlantic, particularly during JJ and in the western Pacific, far from the Sahel. There is also weak warming in part of the western Indian Ocean basin. We also find that the mean upper tropospheric temperature anomaly in the global tropics is anomalously negative for the ENWS composite and anomalously positive for the ENDS composite (not shown).

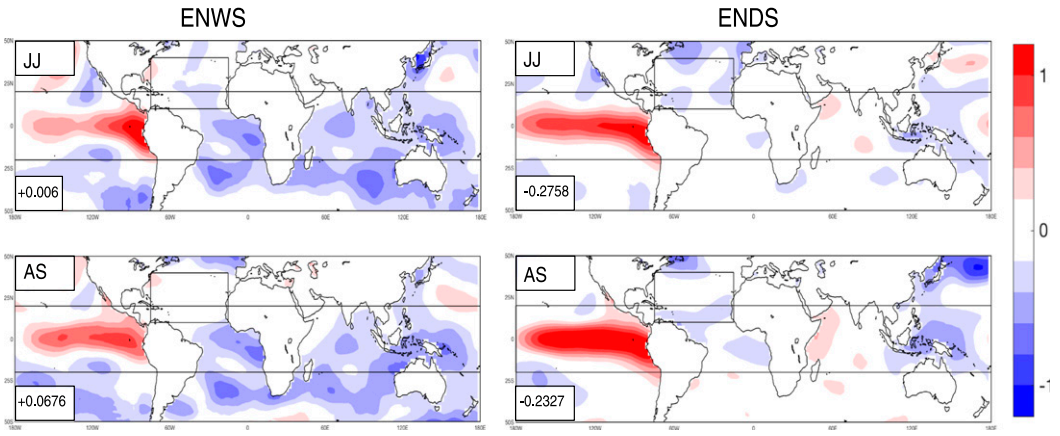


FIG. 5. Average SST anomalies (°C) for (top) JJ and (bottom) AS in the (left) ENWS and (right) ENDS composites. The average value of the NA-GTI is shown in the bottom-left corner for each composite. The black lines distinguish the regions that compose this index: a subtropical North Atlantic box and the global tropics latitudes.

This supports the notion that these contrasting SST patterns, with a very warm Pacific and cold rest of the tropics in the ENWS composite, absent in the ENDS composite, impart a very different influence on the atmospheric column over West Africa. Despite El Niño's presence in both composites, the average temperature profile shows cooling aloft dominating the tropics for the ENWS composite, while warming aloft dominates for the ENDS composite, thus implying a more stable atmospheric profile (not shown).

We find agreement between SST in the various parts of the global ocean and the sign of the observed precipitation anomaly in the Sahel, when we digest the information in Fig. 5 into a single index: the difference between the North Atlantic average and the average over global tropical oceans [following Giannini et al. (2013) with regions specified by the boxes drawn in Fig. 5]. The numeric values indicated in the bottom left of each panel in Fig. 5 give the average of this index; in both early and late parts of the ENWS (ENDS) season, the index value is positive (negative), consistent with the finding that this index helps reconcile Sahel precipitation variability on multiple time scales (Giannini et al. 2013). Here, we see the relevance of this index in a specific subset of years: those years with El Niño occurrence. Note that the influence of the Indian Ocean is considered in our determination of what provides the modulating factor to El Niño when understanding Sahel precipitation variability. The value of the NA-GTI provides an indication of whether the subtropical North Atlantic Ocean is relatively warmer or cooler than the entire global tropical ocean band (thereby encompassing the extent of the Atlantic, Pacific, and Indian Oceans across the tropics).

Next, Fig. 6 shows the frequency of occurrence of warm and cool SST anomalies in each 2.0° by 2.0° grid area for the respective years composing each composite. In the ENWS composite, there are consistent cool anomalies throughout the global tropics (outside the Niño region) with many grid points reporting cool anomalies in five or six of the six years composing the composite. This is especially true in the subtropical South Atlantic Ocean and the Indian Ocean, which when cool favors an enhanced monsoon over the African continent and greater precipitation (Bader and Latif 2003; Dyer et al. 2017) in the Sahel. In the North Atlantic, there is less consistency in terms of the sign of anomalies. Furthermore, in AS for the ENWS composite, there is a split between warm and cool anomalies (three years for each) directly off the coast of West Africa around 15°N. Still, this pattern indicates a weakening of the cool temperatures in JJ that extend throughout this region earlier in the season and may be one reason why the precipitation anomaly map shows wetter conditions later in the season than earlier in the season. In contrast, this same region of the Atlantic shows cool conditions in 5/6 years in the ENDS composite. In addition, there are fewer grid boxes south of the equator in the Atlantic that show anomalously cool conditions in the ENDS composite relative to the ENWS composite, and in the Indian Ocean grid boxes are more often warm (five or six years) than cool.

### *d. Likelihood of below normal Sahel rainfall during El Niño years*

In the left panels of Fig. 7, the observed precipitation values for JJ and AS in all years 1950–2015 are plotted against the value of the subtropical NA-GTI and categorized by type of year: ENWS (blue), ENDS (red), or neither (black). The positive slope of the relationship between precipitation anomalies and the proposed index is consistent with correlations reported in Table 2 and previous findings, when the index was studied in

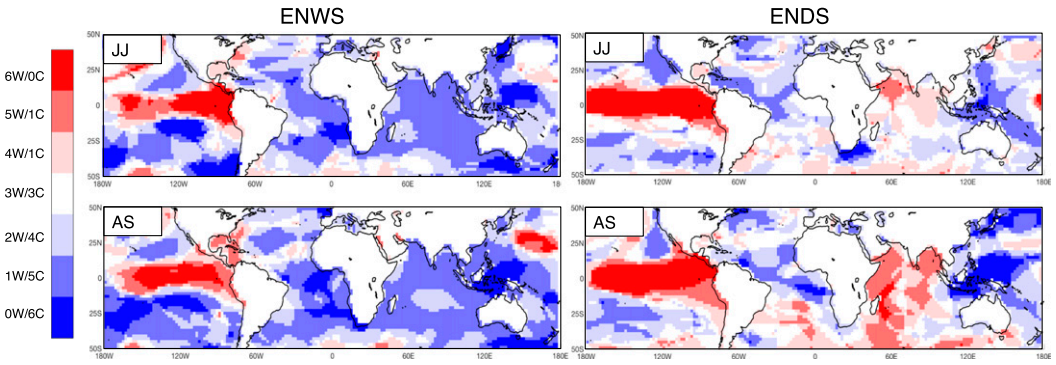


FIG. 6. Frequency of occurrence of warm and cool SST anomalies in each 2.0° by 2.0° grid box for the years composing each composite. The color bar denotes warm or cool SST occurrence for each composite (e.g., "6W/0C" indicates 6 warm years and 0 cool years; "5W/1C" indicates 5 warm years and 1 cool year, and so on for the years composing each composite; $n = 6$ in both cases).

climate models participating in the Climate Model Intercomparison Project (CMIP) (Giannini et al. 2013). In most AS cases, the ENWS years (blue dots) lie to the right of the 0 line, indicating that they tend to occur when the index is positive. In JJ, however, this is not the case (only two of six wet events occur with positive index), which also may help reconcile the feebler positive precipitation anomalies early in the season shown in Fig. 3.

The positive slope between precipitation and the NA-GTI in the left two panels of Fig. 7 is a clear departure from what is shown in the right panels. These latter panels show the same standardized precipitation anomalies plotted against the strength of the Niño-3.4 index. In these panels, there is no clear indication of slope, suggesting that there is not a strong relationship between the strength of the El Niño event itself and the resulting precipitation anomaly signature.

Because of the limited sample size in the observational study, in Fig. 8 we employ output from a suite of SST-forced atmospheric general circulation model experiments. Here we explore the relative likelihood of dry conditions to occur, given the value of the NA-GTI.

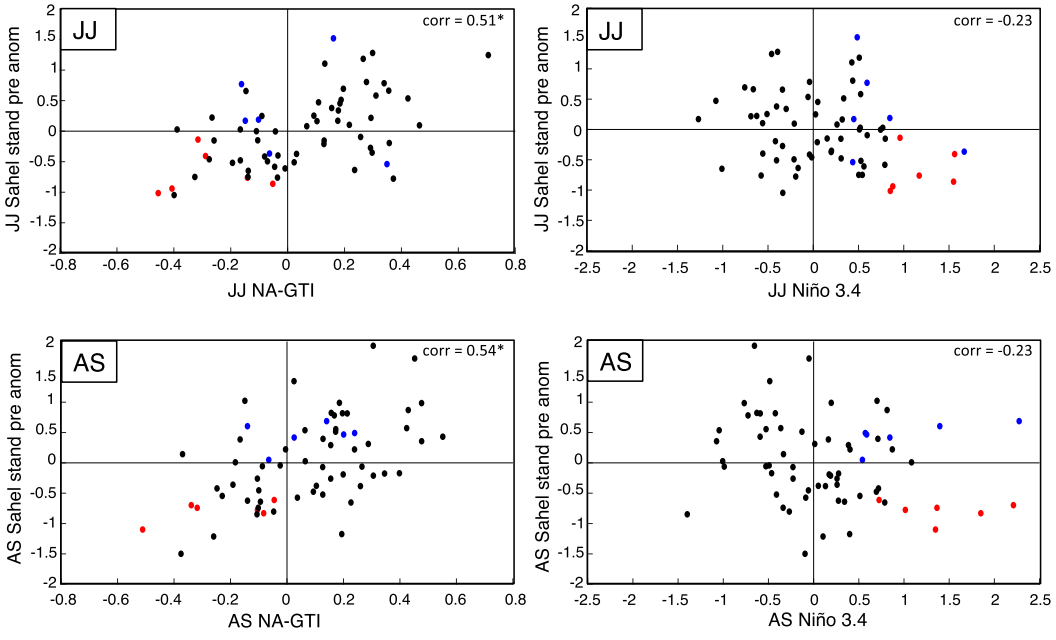


FIG. 7. The (top) JJ and (bottom) AS West African Sahel standardized precipitation anomalies and (left) NA-GTI or (right) Niño-3.4 index. Blue dots indicate years in the ENWS composite, red dots indicate years in the ENDS composite, and black dots are non–El Niño years. Note the differences in the $x$ axes between the two columns. Correlations are listed in the top-right corner of each panel, with an asterisk indicating significance of correlations at $\alpha = 0.05$.

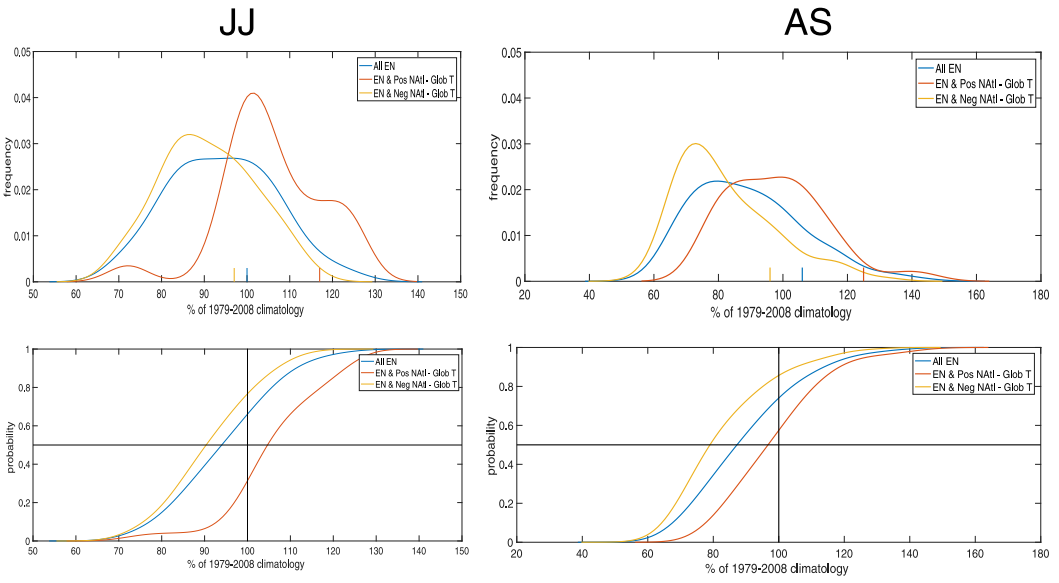


FIG. 8. (top) Probability density functions and (bottom) cumulative distribution functions fit using precipitation output from all CAM5 ensemble members ($n$ = 16) and El Niño events for 1950–2015 ($n$ = 12) for (left) JJ and (right) AS. The blue curve indicates the distribution for all El Niño events and all ensemble members, the red curve indicates the distribution for El Niño years and positive NA-GTI, and the yellow curve indicates the distribution for El Niño years and negative NA-GTI. The average observed precipitation rate (GPCC) is shown as a vertical line along the bottom of the PDFs for all El Niño events (blue), El Niño events and positive NA-GTI (red), and El Niño events and negative NA-GTI (yellow). Note the difference in horizontal scale for the JJ and AS panels.

Simulated precipitation output from the Community Atmospheric Model version 5 (CAM5), forced with historic SSTs from 1856 to 2016 in what is referred to as a GOGA (global ocean–global atmosphere) setup (Pomposi et al. 2015, 2016) is presented. There are 16 such model runs, each starting from different atmospheric initial conditions, making for independent simulations aside from what is uniquely determined by the SST forcing. Figure 8 shows probability distribution function (PDF) curves fitted to the model-simulated Sahel rainfall output selected based on El Niño occurrence and the sign of the NA-GTI. While both JJ and AS months show appreciable shifts in the probability density function when El Niño and positive NA-GTI is compared to El Niño and negative NA-GTI, the differences are greater in the AS case as indicated by the left tails not overlapping in the corresponding PDF. Based on the model output, in JJ when El Niño occurs and the NA-GTI is positive, the probability of the West African Sahel receiving less than climatologic rainfall is only approximately 30% while it is over 70% for the same part of the season when the index is negative. These probabilities change to just over 50% and 80% by AS when the index is positive and negative, respectively. The vertical lines along the $x$ axis of the top panels of Fig. 8 also show the observed precipitation rates for each of the composites from GPCC and clearly show the tendency of the area to receive above-normal precipitation when El Niño occurs and the North Atlantic is anomalously warm compared to the tropics overall. The CDFs display the probability of precipitation to be above or below 100% of the 1979–2008 climatologic value. Consistent with the PDF curves, the CDFs indicate that for JJ, there is a higher probability (~75%) of the Sahel receiving less than climatologic rainfall when it is an El Niño year and the NA-GTI is negative and a much lower probability (~30%) of the same happening in an El Niño year when the NA-GTI is positive. By AS, the probabilities are about 85% for the Sahel to receive less than climatologic rainfall when it is an El Niño year and the NA-GTI is negative and about 50% when it is an El Niño year and the NA-GTI is positive.

Figure 9 provides an overview of various components of the atmospheric circulation anomalies (anomalies of 925-hPa horizontal winds, column-integrated moisture convergence, and sea level pressure) in the two composites and within the season. It is clear that an entirely different circulation pattern emerges in the presence of the different ocean configurations previously described for the two composites (Fig. 5), despite the similar moisture convergence patterns emerging in the tropical Pacific and consistent with El Niño. In JJ and AS for the ENWS composite, there is a weakening of sea level pressure (SLP) over much of the North Atlantic basin. The lower surface pressure over the North Atlantic is consistent with

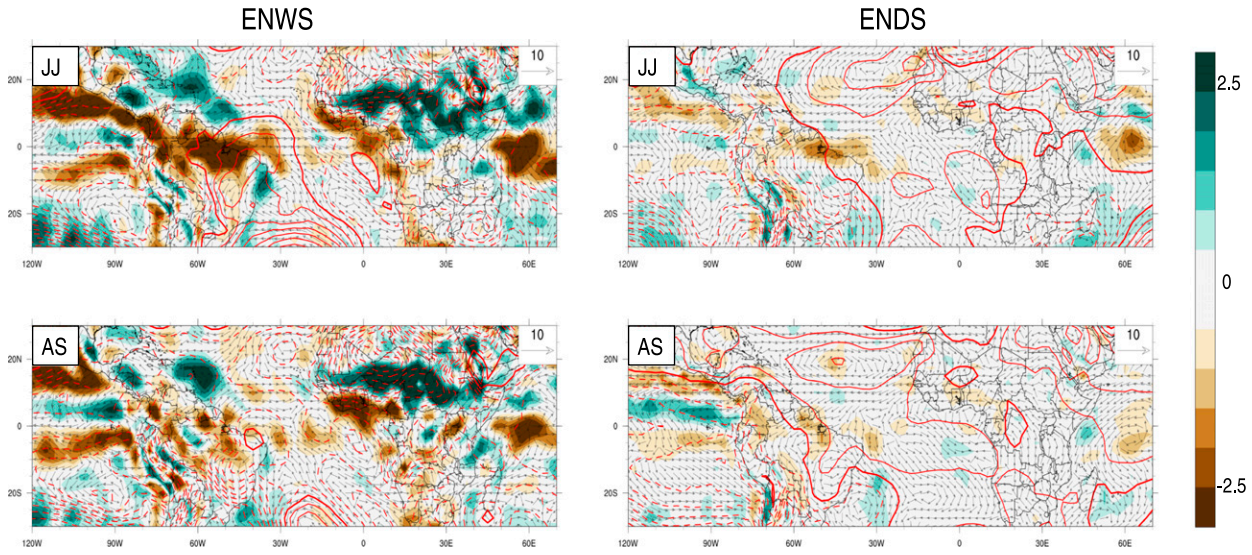


FIG. 9. The (top) JJ and (bottom) AS anomalies of 925-hPa horizontal wind (vectors), column-integrated moisture convergence (colors; mm day$^{-1}$), and SLP (contours; hPa). Data are from the NCEP–NCAR reanalysis. The SLP contours are from −2.5 to 2.5 by 0.5, with positive and negative values indicated by solid and dashed contours, respectively. The zero contour is indicated by the thick red line.

previous studies reporting that a weakened North Atlantic subtropical high corresponds with longer and thereby wetter Sahel seasons (Zhang and Cook 2014). While the response in the JJ horizontal wind anomalies is not as clear, by AS there is increased anomalous westerly flow between 10° and 20°N in the Atlantic consistent with a reduction in SLP and anomalous anticyclonic flow. Such an increased westerly component at low atmospheric levels that derives its origin over the Atlantic has been shown to provide West Africa with additional moisture and result in a wetter Sahel (Fontaine 2003; Lélé et al. 2015; Pu and Cook 2010, 2012). This is consistent with the patterns shown in Fig. 9 and the band of anomalous positive moisture convergence (colors).

On the other hand, in the JJ composite associated with the ENDS, there is a strengthening of SLP centered off the west coast of Africa between about 20°–30°N and 10°–30°W. By AS, the SLP anomalies in this same region strengthen further, with anomalous easterly flow from the African continent along the southern margin of the large-scale anticyclonic flow pattern that develops and a lack of moisture convergence over the Sahel. In summary, these figures point to a redistribution of pressure and convergence patterns, as well as moisture flow into the region that are distinctly different between the two composites. These appear consistent with differences in the global SST field, particularly in the Atlantic, the source from which the monsoon derives its moisture. Associated differences in SLP are also shown over the African continent, with a strengthening of the thermal low in the ENWS composite (indicated by the negative SLP anomalies) and a weakening of the low (indicated by the positive SLP anomalies) in the ENDS composite.

The lack of symmetry in the magnitude of the atmospheric fields compared to the precipitation fields is likely due to the ways in which the different basins are theorized to influence the Sahel. For example, Pomposi et al. (2016) show that the primarily impact of ENSO on the Sahel is through an influence of the large-scale circulation pattern (and a Gill–Matsuno-type response to heating), which drives moisture away from the continent, as seen by the stronger wind anomalies in Fig. 9 in the ENDS composites. This circulation feature is consistent from east to west across the entire Sahel, helping to explain the extent of the dry band stretching from one end of the continent to another. On the other hand, the Atlantic influence is primarily through establishing additional moisture supply via westerly wind flow and the enhanced moisture content of the air when the northern Atlantic is anomalously warm (e.g., Pomposi et al. 2015). This can be seen in Fig. 9 in the ENWS panels, with weaker wind anomalies emanating from the ocean, but important for the additional moisture convergence (also impacted by the SLP anomalies via circulation response) primarily over the western Sahel. In this way, the lack of east–west symmetry of the wet signal is consistent with the theory of Atlantic influence on the region and the results presented in Fig. 9.

## 4. Discussion and conclusions

Motivated by the historic El Niño event of 2015 and the surprising behavior in West African Sahel precipitation

during that summer, this study has provided an observational examination of Sahel precipitation diversity during recent El Niño events. We study average Sahel summer (JJAS) precipitation in 12 El Niño years that occurred since 1950. The standardized observed precipitation in the Sahel is anomalously high in 6 of the 12 years and anomalously low in the remaining 6 years. We then composite around the precipitation signal, designating an El Niño/wet Sahel (ENWS) composite and an El Niño/dry Sahel (ENDS) composite based on JJAS behavior but detail early-season (JJ) and late-season (AS) behavior. Anomalously wet conditions in the ENWS composite are confined to the westernmost part of West Africa, west of about 0° longitude. The rainfall anomalies are much stronger later in the season, around +0.8 standardized units than earlier in the season (between +0.4 and +0.6). Notably, however, when the composite view is taken the dichotomy between early-season drying and late-season wetting shown for 2015 (Fig. 1) disappears. This is in line with JJ precipitation behavior that does not as consistently show positive precipitation anomalies when regionally averaged (only 4/6 ENWS years have above normal precipitation anomalies in JJ whereas 6/6 do for AS; see Fig. S1 in the online supplemental material). Projections of climate change in the Sahel indicate that the early season is most consistently getting drier, whereas the late season is getting wetter (Biasutti and Sobel 2009). It is interesting that the sole ENWS year after 2000 explored here also clearly shows this same behavior. In contrast, we find that for the ENDS composite there is consistent and coherent drying both north to south and east to west across the extent of the Sahel with reduced precipitation rates that are approximately similar both early and later in the season. Furthermore, there is clearer consistency in the sign of anomalies in the ENDS composite, with between 5 and 6 of the total 6 years showing drying at each grid box by AS.

We next ask ourselves what helps to distinguish wet from dry El Niño years. We turn our attention to the configuration of the global ocean, reflecting the current understanding that many different basins may impact year-to-year variability in Sahel precipitation. Even though all selected years are El Niño years, the two composites show some slight differences in the SST pattern in the tropical Pacific. Specifically, the El Niño signal is stronger in the ENDS composite than in the ENWS composite. However, from our results, we find a compelling argument for reconciling an anomalously wet and dry Sahel during El Niño years by referencing an index that relates a local basin—the subtropical North Atlantic—to the overall pattern in the global tropical oceans that includes the El Niño pattern. The subtropical NA-GTI has been shown to reconcile precipitation variability in the Sahel over the twentieth and twenty-first centuries as well as in CMIP projections for the future (Giannini et al. 2013).

Consideration of the NA-GTI also takes into account longer-term variations inherent in the climate system and known to be important for Sahel rainfall variability. The interference of different time scales of variability, evident in Fig. 2, is in line with previous understanding of the influences of the Atlantic and Pacific basins on Sahel precipitation variability. The former acts as a supplier of moisture to the region, and variations in SST affect moisture transport and convergence over land (Giannini et al. 2008, 2013; Pomposi et al. 2015; Lélé et al. 2015; Pu and Cook 2012), whereas the latter influences the vertical stability of the atmosphere over the Sahel and provides conditions favorable for convection to set up or not (Janicot et al. 1996; Hagos and Cook 2008). The Atlantic displays a large low-frequency, decadal-to-multidecadal variability component that affects Sahel precipitation variability, whereas the Pacific imprints its influence in the region on a faster, interannual time scale. Thus, the slow Atlantic impact modulates the fast El Niño impact, enhancing the El Niño–forced drying of the Sahel when it is cold with respect to SST in the global tropics and attenuating the El Niño impact when it is warm.

We suggest that a positive NA-GTI indicates that increased moisture supply from the Atlantic overcomes a convective threshold set in the tropics, while a negative index implies that the threshold is not met. In our composites, there is agreement in terms of the sign of the index with this hypothesis. The sign is (weakly) positive in JJ for the ENWS composite and becomes more strongly positive in AS when the positive precipitation anomalies are also their largest. A large contributor to the positive index in the ENWS composite is the cold anomalies in the global tropics (outside the Niño-3.4 region) particularly in the Indian Ocean, which is very consistent among the years composing the composite. As reported in previous work, a colder than normal Indian Ocean helps to establish a more vigorous flow of moisture from the Atlantic into Africa (Bader and Latif 2003; Dyer et al. 2017). Additionally, advection of air from the subtropical North Atlantic feeds the Sahel with increased moisture and destabilizes the atmospheric column (Pu and Cook 2012; Hastenrath and Polzin 2011). The increased westerly flow over the subtropical North Atlantic shown in the ENWS composites is consistent with a weakening of the Atlantic subtropical anticyclone and weakened SLP in response to SST changes (Kushnir et al. 2010). Locally, the response in the Sahel to this global oceanic anomaly pattern is anomalous rising

air that is consistent with a deeper than normal monsoon low, enhanced westerly flow, and positive precipitation anomalies over the region. This situation is in clear contrast to the ENDS composite, when the NA-GTI is negative. In this case, anomalous easterly flow away from the Sahel is consistent with the increased subsidence found in direct response to El Niño forcing (Pomposi et al. 2016). Additionally, the warm Indian Ocean in this case also imparts flow that causes moisture flux away from the Sahel (Hagos and Cook 2008) and amplifies the El Niño pattern of anomalous subsidence and the associated divergence of moisture there.

Last, we fit distribution curves to model output based once more on the two SST indicators (NA-GTI and Niño-3.4). Shifts in the probability density functions indicate that the likelihood of the Sahel receiving less than climatologic precipitation when the NA-GTI is positive during El Niño is only about 30% and 50% for JJ and AS, respectively, compared with about 70% and over 80% when the NA-GTI is negative during El Niño.

Overall, the present work provides compelling evidence that the traditionally viewed negative correlation between precipitation in the Sahel and ENSO must be considered carefully in concert with other regional and global influences. This finding is akin to previous work understanding the occurrence of drought in the presence of ENSO and additional oceanic variability in the southwestern United States. Results there indicate that drought varies in concert with ENSO and Atlantic multidecadal variability (AMV), with clear differences in drought occurrence when AMV is positive or negative (Kushnir et al. 2010). In this work, we show that multidecadal changes across the globe can modulate the influence of warm ENSO events in another semiarid region of interest, the West African Sahel. Our results point to an important role of the North Atlantic in supplying additional moisture to the Sahel when the northern part of the basin is anomalously warm relative to the southern part of the basin. There is also evidence here for a role of the Indian Ocean basin, particularly in switching from displaying anomalously cool conditions early in the twentieth century to anomalously warm conditions more recently. Our results are similar to the conclusions of recent published work by Suárez-Moreno et al. (2018), who also show that underlying modes of SST variability can inhibit or enhance interannual teleconnections understood to influence Sahel summertime precipitation. To more fully attribute the relative role of each basin in overcoming the El Niño influence on Sahel precipitation in the current work, a complete suite of idealized model experiments with multiple ensemble members is necessary. In such idealized setting, SST anomalies can be applied in different ocean basins, their strengths varied, and the resulting evolution of convection studied with high temporal resolution. This is the goal of future research.

The present work serves as one important case study for scientists and forecasters in the Sahel to consider in El Niño years when information from seasonal forecasts is disseminated locally. The results presented here are especially timely as efforts to provide seasonal forecasts of precipitation and additional climate information to guide decision makers have been steadily increasing in recent decades (Tall 2013). In the summer of 2015, it is estimated that approximately 3.5 million farmers in Senegal alone received forecasts for the rainy season (O. Ndiaye 2015, personal communication). Such forecasts exploit the predictability of the global ocean and, in particular, of the phase and strength of ENSO. Thus, a study that illustrates how different Sahel precipitation signatures can exist during El Niño and that helps to identify how other basins may interfere with the signal from the Pacific to change the relative risk of anomalously low precipitation in the Sahel is of great use for users of climate information in the region. Furthermore, several recent studies that document existing skill in SST forecasts for parts of the Atlantic basin (Zanna 2012; Chang et al. 2003; Hu et al. 2013) indicate that the changes we see consistent with rainfall response in the Sahel may also be incorporated months in advance of the season to provide useful forecasting information prior to the first rains occurrence.

*Acknowledgments.* We thank Donna Lee at the Lamont-Doherty Earth Observatory for running the CAM5 experiments used in this study. We also acknowledge the efforts of Naomi Henderson to maintain these data for scientific research use. The paper was improved through thoughtful comments and discussions with Ben Lintner, Ousmane Ndiaye, Adam Sobel, and Katy Sheen. We thank three anonymous reviewers for thoughtful suggestions that improved the paper. This research was funded in part by an award from the U.S. National Science Foundation AGS-1612904. The GPCC, CRU, GPCP, and ERSST data were retrieved from the International Research Institute for Climate and Society (IRI) Data Library (http://iridl.ldeo.columbia.edu). The GOGA CAM5 and NCEP–NCAR reanalysis data were accessed through the Lamont-Doherty Earth Observatory Ocean and Climate Physics Division Data Library (http://kage.ldeo.columbia.edu:81). This paper is Lamont-Doherty Earth Observatory Publication No. 8364.

## REFERENCES

Adler, R. F., and Coauthors, 2003: The version-2 Global Precipitation Climatology Project (GPCP) monthly precipitation analysis (1979–present). *J. Hydrometeor.*, **4**, 1147–1167, https://doi.org/10.1175/1525-7541(2003)004<1147:TVGPCP>2.0.CO;2.

Ali, A., A. Amani, A. Diedhiou, and T. Lebel, 2005: Rainfall estimation in the Sahel. Part II: Evaluation of rain gauge networks in the CILSS countries and objective intercomparison of rainfall products. *J. Climate*, **44**, 1707–1722, https://doi.org/10.1175/JAM2305.1.

Bader, J., and M. Latif, 2003: The impact of decadal-scale Indian Ocean sea surface temperature anomalies on Sahelian rainfall and the North Atlantic Oscillation. *Geophys. Res. Lett.*, **30**, 2169, https://doi.org/10.1029/2003GL018426.

Becker, A., P. Finger, A. Meyer-Christoffer, B. Rudolf, K. Schamm, U. Schneider, and M. Ziese, 2013: A description of the global land-surface precipitation data products of the Global Precipitation Climatology Centre with sample applications including centennial (trend) analysis from 1901–present. *Earth Syst. Sci. Data*, **5**, 71–99, https://doi.org/10.5194/essd-5-71-2013.

Biasutti, M. and A. H. Sobel, 2009: Delayed Sahel rainfall and global seasonal cycle in a warmer climate. *Geophys. Res. Lett.*, **36**, L23707, https://doi.org/10.1029/2009GL041303.

——, I. M. Held, A. H. Sobel, and A. Giannini, 2008: SST forcings and Sahel rainfall variability in simulations of the twentieth and twenty-first centuries. *J. Climate*, **21**, 3471–3486, https://doi.org/10.1175/2007JCLI1896.1.

Chang, P., Saravanan, R., and L. Ji, 2003: Tropical Atlantic seasonal predictability: The roles of El Niño remote influence and thermodynamic air-sea feedback. *Geophys. Res. Lett.*, **30**, 1501, https://doi.org/10.1029/2002GL016119.

Chiang, J. C. H., and A. H. Sobel, 2002: Tropical tropospheric temperature variations caused by ENSO and their influence on the remote tropical climate. *J. Climate*, **15**, 2616–2631, https://doi.org/10.1175/1520-0442(2002)015<2616:TTTVCB>2.0.CO;2.

Dyer, E. L. E., D. B. A. Jones, R. Li, H. Sawaoka, and L. Mudryk, 2017: Sahel precipitation and regional teleconnections with the Indian Ocean. *J. Geophys. Res.*, **122**, 5654–5676, https://doi.org/10.1002/2016JD026014.

Folland, C. K., T. N. Palmer, and D. E. Parker, 1986: Sahel rainfall and worldwide sea temperatures 1901–85. *Nature*, **320**, 602–607, https://doi.org/10.1038/320602a0.

Fontaine, B., 2003: Atmospheric water cycle and moisture fluxes in the West African monsoon: Mean annual cycles and relationship using NCEP/NCAR reanalysis. *Geophys. Res. Lett.*, **30**, 1117, https://doi.org/10.1029/2002GL015834.

Gaetani, M., B. Fontaine, P. Roucou, and M. Baldi, 2010: Influence of the Mediterranean Sea on the West African monsoon: Intraseasonal variability in numerical simulations. *J. Geophys. Res.*, **115**, D24115, https://doi.org/10.1029/2010JD014436.

Giannini, A., and A. Kaplan, 2019: The role of aerosols and greenhouse gases in Sahel drought and recovery. *Climatic Change*, **152**, 449–466, https://doi.org/10.1007/s10584-018-2341-9.

——, R. Saravanan, and P. Chang, 2003: Oceanic forcing of Sahel rainfall on interannual to interdecadal time scales. *Science*, **302**, 1027–1030, https://doi.org/10.1126/science.1089357.

——, M. Biasutti, I. M. Held, and A. H. Sobel, 2008: A global perspective on African climate. *Climatic Change*, **90**, 359–383, https://doi.org/10.1007/s10584-008-9396-y.

——, S. Salack, T. Lodoun, A. Ali, A. T. Gaye, and O. Ndiaye, 2013: A unifying view of climate change in the Sahel linking intra-seasonal, interannual and longer time scales. *Environ. Res. Lett.*, **8**, 024010, https://doi.org/10.1088/1748-9326/8/2/024010.

Gill, A. E., 1980: Some simple solutions for heat-induced tropical circulation. *Quart. J. Roy. Meteor. Soc.*, **106**, 447–462, https://doi.org/10.1002/qj.49710644905.

Hagos, S. M., and K. H. Cook, 2008: Ocean warming and late twentieth-century Sahel drought and recovery. *J. Climate*, **21**, 3797–3814, https://doi.org/10.1175/2008JCLI2055.1.

Harris, I., P. D. Jones, T. J. Osborn, and D. H. Lister, 2014: Updated high-resolution grids of monthly climatic observations—The CRU TS3.10 dataset. *Int. J. Climatol.*, **34**, 623–642, https://doi.org/10.1002/joc.3711.

Hastenrath, S., and D. Polzin, 2011: Long-term variations of circulation in the tropical Atlantic sector and Sahel rainfall. *Int. J. Climatol.*, **31**, 649–655, https://doi.org/10.1002/joc.2116.

Hu, Z.-Z., A. Kumar, B. Huang, W. Wang, J. Zhu, and C. Wen, 2013: Prediction skill of monthly SST in the North Atlantic Ocean in NCEP Climate Forecast System version 2. *Climate Dyn.*, **40**, 2745–2759, https://doi.org/10.1007/s00382-012-1431-z.

Huang, B., and Coauthors, 2015: Extended reconstructed sea surface temperature version 4 (ERSST.v4). Part I: Upgrades and intercomparisons. *J. Climate*, **28**, 911–930, https://doi.org/10.1175/JCLI-D-14-00006.1.

Janicot, S., V. Moron, and B. Fontaine, 1996: Sahel droughts and ENSO dynamics. *Geophys. Res. Lett.*, **23**, 515–518, https://doi.org/10.1029/96GL00246.

——, S. Trzaska, and I. Poccard, 2001: Summer Sahel–ENSO teleconnection and decadal time scale SST variations. *Climate Dyn.*, **18**, 303–320, https://doi.org/10.1007/s003820100172.

Joly, M., and A. Voldoire, 2009: Influence of ENSO on the West African monsoon: Temporal aspects and atmospheric processes. *J. Climate*, **22**, 3193–3210, https://doi.org/10.1175/2008JCLI2450.1.

Kalnay, E., and Coauthors, 1996: The NCEP/NCAR 40-Year Reanalysis Project. *Bull. Amer. Meteor. Soc.*, **77**, 437–471, https://doi.org/10.1175/1520-0477(1996)077<0437:TNYRP>2.0.CO;2.

Kushnir, Y., R. Seager, M. Ting, N. Naik, and J. Nakumura, 2010: Mechanisms of tropical Atlantic SST influence on North American precipitation variability. *J. Climate*, **23**, 5610–5628, https://doi.org/10.1175/2010JCLI3172.1.

Lamb, P. J., 1978: Large-scale tropical Atlantic surface circulation patterns associated with sub-Saharan weather anomalies. *Tellus*, **30**, 240–251, https://doi.org/10.3402/tellusa.v30i3.10338.

Lélé, M. I., L. M. Leslie, and P. J. Lamb, 2015: Analysis of low-level atmospheric moisture transport associated with the West African monsoon. *J. Climate*, **28**, 4414–4430, https://doi.org/10.1175/JCLI-D-14-00746.1.

Lintner, B. R., and J. C. H. Chiang, 2005: Reorganization of tropical climate during El Niño: A weak temperature gradient approach. *J. Climate*, **18**, 5312–5329, https://doi.org/10.1175/JCLI3580.1.

Lu, J., 2009: The dynamics of the Indian Ocean sea surface temperature forcing of Sahel drought. *Climate Dyn.*, **33**, 445–460, https://doi.org/10.1007/s00382-009-0596-6.

Lyon, B., 2004: The strength of El Nino and the spatial extent of tropical drought. *Geophys. Res. Lett.*, **31**, L21204, https://doi.org/10.1029/2004GL020901.

Neale, R. B., and Coauthors, 2012: Description of the NCAR Community Atmosphere Model (CAM 5.0). NCAR Tech. Note NCAR/TN-486+STR, 274 pp., http://www.cesm.ucar.edu/models/cesm1.0/cam/docs/description/cam5_desc.pdf.

Neelin, J. D., C. Chou, and H. Su, 2003: Tropical drought regions in global warming and El Niño teleconnections. *Geophys. Res. Lett.*, **30**, 2275, https://doi.org/10.1029/2003GL018625.

Nicholson, S., and P. J. Webster, 2007: A physical basis for the interannual variability of rainfall in the Sahel. *Quart. J. Roy. Meteor. Soc.*, **133**, 2065–2084, https://doi.org/10.1002/qj.104.

——, and Coauthors, 2003: Validation of TRMM and other rainfall estimates with a density gauge dataset for West Africa. Part I: Validation of GPCC rainfall product and pre-TRMM satellite and blended products. *J. Appl. Meteor.*, **42**, 1337–1354, https://doi.org/10.1175/1520-0450(2003)042<1337:VOTAOR>2.0.CO;2.

Palmer, T. N., 1986: Influence of the Atlantic, Pacific and Indian Oceans on Sahel rainfall. *Nature*, **322**, 251–253, https://doi.org/10.1038/322251a0.

Park, J.-Y., J. Bader, and D. Matei, 2016: Anthropogenic Mediterranean warming essential driver for present and future Sahel rainfall. *Nat. Climate Change*, **6**, 941–945, https://doi.org/10.1038/nclimate3065.

Pomposi, C., Y. Kushnir, and A. Giannini, 2015: Moisture budget analysis of SST-driven decadal Sahel precipitation variability in the twentieth century. *Climate Dyn.*, **44**, 3303–3321, https://doi.org/10.1007/s00382-014-2382-3.

——, A. Giannini, Y. Kushnir, and D. E. Lee, 2016: Understanding Pacific Ocean influence on interannual precipitation variability in the Sahel. *Geophys. Res. Lett.*, **43**, 9234–9242, https://doi.org/10.1002/2016GL069980.

Pu, B., and K. H. Cook, 2010: Dynamics of the West African westerly jet. *J. Climate*, **23**, 6263–6276, https://doi.org/10.1175/2010JCLI3648.1.

——, and ——, 2012: Role of the West African westerly jet in Sahel rainfall variations. *J. Climate*, **25**, 2880–2896, https://doi.org/10.1175/JCLI-D-11-00394.1.

Rowell, D. P., 2003: The impact of Mediterranean SSTs on the Sahelian rainfall season. *J. Climate*, **16**, 849–861, https://doi.org/10.1175/1520-0442(2003)016<0849:TIOMSO>2.0.CO;2.

——, C. K. Folland, K. Maskell, J. A. Owen, and M. N. Ward, 1992: Modelling the influence of global sea surface temperatures on the variability and predictability of seasonal Sahel rainfall. *Geophys. Res. Lett.*, **19**, 905–908, https://doi.org/10.1029/92GL00939.

——, ——, ——, and M. N. Ward, 1995: Variability of summer rainfall over tropical north Africa (1906–92): Observations and modeling. *Quart. J. Roy. Meteor. Soc.*, **121**, 669–704, https://doi.org/10.1002/qj.49712152311.

Seth, A., S. A. Rauscher, M. Rojas, A. Giannini, and S. J. Camargo, 2011: Enhanced spring convective barrier for monsoons in a warmer world? *Climatic Change*, **104**, 403–414, https://doi.org/10.1007/s10584-010-9973-8.

Sheen, K. L., D. M. Smith, N. J. Dunstone, R. Eade, D. P. Rowell, and M. Vellinga, 2017: Skillful prediction of Sahel summer rainfall on inter-annual and multi-year timescales. *Nat. Commun.*, **8**, 14966, https://doi.org/10.1038/ncomms14966.

Suárez-Moreno, R., B. Rodriguez-Fonseco, J. A. Barroso, and A. H. Fink, 2018: Interdecadal changes in the leading ocean forcing of Sahelian rainfall interannual variability: Dynamics and role of multidecadal SST background. *J. Climate*, **31**, 6687–6710, https://doi.org/10.1175/JCLI-D-17-0367.1.

Tall, A., 2013: What are climate services? *WMO Bull.*, **62**, (special issue), 7–11, https://public.wmo.int/en/bulletin/what-do-we-mean-climate-services.

Thiaw, W. M., A. G. Barnston, and V. Kumar, 1999: Predictions of African rainfall on the seasonal timescale. *J. Geophys. Res.*, **104**, 31 589–31 597, https://doi.org/10.1029/1999JD900906.

Ward, M. N., 1998: Diagnosis and short-lead time prediction of summer rainfall in tropical North Africa at interannual and multidecadal timescales. *J. Climate*, **11**, 3167–3191, https://doi.org/10.1175/1520-0442(1998)011<3167:DASLTP>2.0.CO;2.

Yulaeva, E., and J. M. Wallace, 1994: The signature of ENSO in global temperature and precipitation fields derived from the Microwave Sounding Unit. *J. Climate*, **7**, 1719–1736, https://doi.org/10.1175/1520-0442(1994)007<1719:TSOEIG>2.0.CO;2.

Zanna, L., 2012: Forecast skill and predictability of observed Atlantic sea surface temperatures. *J. Climate*, **25**, 5047–5056, https://doi.org/10.1175/JCLI-D-11-00539.1.

Zhang, G., and K. H. Cook, 2014: West African monsoon demise: Climatology, interannual variations and relationship to seasonal rainfall. *J. Geophys. Res.*, **119**, 10 175–10 193, https://doi.org/10.1002/2014JD022043.

Zhang, R., and T. Delworth, 2006: Impact of Atlantic multidecadal oscillations on India/Sahel rainfall and Atlantic hurricanes. *Geophys. Res. Lett.*, **33**, L17712, https://doi.org/10.1029/2006gl026267.